Sequential amplitudes in heavy-ion induced two-proton transfer reactions*

P. P. Tung,† K. A. Erb, M. W. Sachs,‡ G. B. Sherwood, R. J. Ascuitto, and D. A. Bromley
A. W. Wright Nuclear Structure Laboratory, Physics Department, Yale University, New Haven, Connecticut 06520
(Received 6 March 1978)

Angular distributions have been measured for the reactions ^{88}Sr(^{16}O,^{14}C)^{90}Zr and ^{90}Zr(^{16}O,^{14}C)^{92}Mo at 80 MeV, and ^{88}Sr(^{12}C,^{10}Be)^{90}Zr and ^{90}Zr(^{12}C,^{10}Be)^{92}Mo at 60 MeV. The data were analyzed with full recoil, coupled-channel Born approximation calculations, in which both direct (one-step) and sequential (two-step) reaction routes were considered. Detailed shell model wave functions were used to construct all form factors. The calculated sequential contributions to the cross sections were found to be significantly larger than those associated with direct transfer, and inclusion of the two-step routes substantially improved agreement with experiment. The calculated angular distribution shapes were found to depend on both the intermediate Q value of the sequential process, and also on the microscopic configurations involved in the transfer. In addition, a previously unreported configuration dependence of the recoil corrections was noted in the calculations.

[NUCLEAR REACTIONS ^{88}Sr(^{16}O, ^{16}O), ^{88}Sr(^{16}O, ^{14}C), ^{90}Zr(^{16}O, ^{16}O), ^{90}Zr(^{16}O, ^{14}C), $E = 80$ MeV; ^{88}Sr(^{12}C, ^{12}C), ^{88}Sr(^{12}C, ^{10}Be), ^{90}Zr(^{12}C, ^{12}C), ^{90}Zr(^{12}C, ^{10}Be), $E = 60$ MeV; enriched targets, measured $\sigma(\theta)$. Finite range DWBA and CCBA analyses of direct and sequential transfer, compared with data.]

I. INTRODUCTION

In almost all heavy-ion, and a large fraction of the light-ion, induced multinucleon transfer reaction studies reported to date it has been assumed that the nucleons involved are transferred simultaneously (as an effective cluster) between the projectile and target involved. The question of the importance of competing reaction amplitudes wherein the nucleons are transferred sequentially via well-defined intermediate nuclear states has remained an open one.

Recent studies of charge-exchange reactions induced by light ions have illustrated the importance of such sequential transfer processes[1-3] and indicated a new direction in transfer reaction study that merits additional attention. Inclusion of sequential processes in the above, and in more recent studies,[4-7] has improved the agreement of calculated with experimental cross sections both in magnitude and in the shapes of the angular distributions. The question of the possible importance of sequential transfer amplitudes in heavy-ion induced reactions, however, remains very much in an exploratory phase although studies in the calcium and nickel regions have suggested[8-9] that including sequential amplitudes in the analysis improves the absolute normalization of reaction model predictions to experiment by factors of 5–10. In the present study we investigate the importance of the sequential mechanism in—and explore the dependence on nuclear structure characteristics of—heavy-ion induced, two-proton transfer reactions on ^{88}Sr and ^{90}Zr targets.

We have selected these targets—having closed neutron shells ($N = 50$)—for such studies both because their small deformations make negligible the effects of higher-order multistep inelastic transfer processes[10] which would have greatly complicated the analyses and perhaps obscured the sequential effects of interest and because sufficiently detailed shell model calculations have been reported[11-17] for this mass region to permit construction of realistic transfer form factors for the direct and sequential processes. The projectile energies available to us did not permit a choice of targets in the lead region; insufficient target nuclei are available in the vicinity of ^{48}Ca, and the ^{40}Ca core is not adequately magic for our purposes. ^{16}O and ^{12}C projectile beams were selected for convenience and because it was hoped that the very different structures involved would lead to observable structure dependent effects in the measured cross sections. As an additional attractive feature we note that heavy-ion induced reactions, even with the projectiles as light as ^{16}O and ^{12}C, have the advantage that semi-classical concepts such as r- and L-space localization, can be used to obtain an understanding of many of the salient features of the experimental data.[18]

Cross sections for the (^{12}C,^{10}Be) and (^{16}O,^{14}C) two-proton transfer reactions were measured for both ^{88}Sr and ^{90}Zr targets, and the experimental data were subjected to full-recoil distorted-wave Born approximation (DWBA) and second-order Born approximation analyses. A number of significant results emerged. First, the predicted configuration dependence of the direct transfer process was found to differ in no-recoil and in full recoil DWBA calculations, thus requiring the more accurate but much more time consuming full-re-

coil treatment in all the analyses reported in this work. Second, we report the first observation of which we are aware of significant sequential amplitude effects dependent upon the microscopic configurations active in the models used. Third, we have observed a significant dependence of the sequential transfer amplitudes on the intermediate reaction Q values. And finally, the systematic trends in the four reactions studied are shown to reflect their sensitive dependence upon reaction mechanisms, underlying nuclear structure, and the binding energies of the transferred nucleon in the projectile-reaction product and the target-residual nucleus systems (the "light" and "heavy" systems, respectively). In addition, an investigation of the relative population of the first two 0^+ states in ^{90}Zr via the reactions ^{88}Sr(^{12}C, ^{10}Be)^{90}Zr and ^{88}Sr(^{16}O, ^{14}C)^{90}Zr served to validate the truncated shell model wave functions used in these analyses.

II. EXPERIMENTAL METHOD

Angular distributions corresponding to the population of low-lying residual states in the reactions ^{88}Sr(^{16}O, ^{14}C)^{90}Zr, ^{90}Zr(^{16}O, ^{14}C)^{92}Mo, ^{88}Sr(^{12}C, ^{10}Be)^{90}Zr, and ^{90}Zr(^{12}C, ^{10}Be)^{92}Mo, and elastic scattering in the respective entrance channels were measured over a center-of-mass angular range from 10° to 70°. These experiments were carried out using the MP-1 tandem Van de Graaff accelerator of the Wright Laboratory with ^{16}O and ^{12}C beams of energies of 80 and 60 MeV, respectively; these energies were selected to be some 10 ~ 15 MeV above the corresponding Coulomb barriers. The targets were prepared[19] by evaporating enriched metal (>98% ^{88}Sr and 97.65% ^{90}Zr) onto carbon backings (of areal densities 20 μg/cm^2 and 40 μg/cm^2 for ^{88}Sr and ^{90}Zr targets, respectively) and were nominally 60 μg/cm^2 thick. An array of three semiconductor surface-barrier detector telescopes successively 10° apart and cooled by thermoelectric devices[20] was used for particle detection and identification.

A typical spectrum for the reaction ^{88}Sr(^{16}O, ^{14}C)^{90}Zr is shown in Fig. 1; the energy resolution in general was about 150 ~ 200 keV full width at half maximum (FWHM). Using this resolution, the low-lying states in the residual nuclei were adequately resolved, except for the $(2^+, 5^-)$ levels near 2.2 MeV excitation in ^{90}Zr (Fig. 1). The predominant contribution to this $(2^+, 5^-)$ peak in ^{90}Zr was found from a subsidiary experiment to arise through population of the 5^- state, which contributed at least 90% of the $(2^+, 5^-)_{\text{total}}$ at the angles measured. This separate experiment was carried out using the quadrupole-dipole-dipole-dipole magnetic spectrometer at the Brookhaven National Laboratory to achieve an energy resolution adequate to resolve

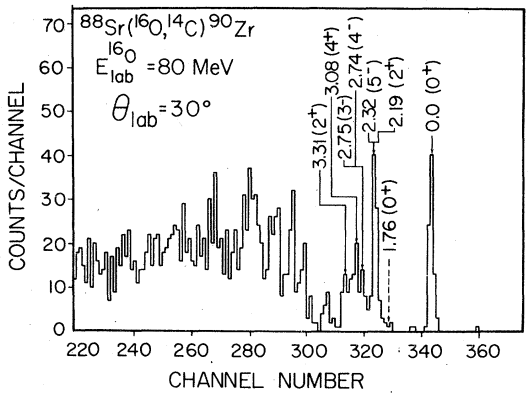

FIG. 1. Spectrum of ^{14}C from the ^{88}Sr(^{16}O, ^{14}C)^{90}Zr reaction at 80 MeV, measured at 30°_{lab}.

the transitions populating these two close-lying residual states. The absolute cross sections were determined by normalizing the transfer reaction yield to the elastic scattering yield at forward angles ($\theta < 15°$), where the latter cross section was assumed to be purely Rutherford in character; they are believed to be accurate to better than ±15%.

It should be noted that no significant reaction yield to the first excited 0^+ state of ^{90}Zr at 1.76 MeV appears in Fig. 1. Inasmuch as the ratio of the populations of this state and the 0^+ ground state provides a sensitive test of the available truncated $[(2p_{1/2})^2, (1g_{9/2})^2]$ wave functions used in our analyses, supplementary studies were carried out involving much longer running times. No statistically significant reaction yield identifiable with the excited 0^+ state was observed; lower limits of 75 and 50 were placed, for the reactions ^{88}Sr(^{12}C, ^{10}Be)^{90}Zr and ^{88}Sr(^{16}O, ^{14}C)^{90}Zr, respectively, on the ratio of the cross sections corresponding to population of the ground and first excited states.

The angular distributions measured for the (^{12}C, ^{10}Be) and (^{16}O, ^{14}C) reactions are shown in Fig. 2.

III. ANALYSES AND RESULTS

Reaction calculations were carried out using the source term method developed by Ascuitto and Glendenning[21] in both the full-recoil first-order DWBA, with two nucleons transferred simultaneously, and in the full-recoil second-order Born approximation with the two nucleons transferred sequentially. The computer code used was LISA[22] with substantial additions[23] necessary to permit a full-recoil treatment.

The analyses utilized the full-recoil for reasons that will be discussed in subsection A. The effects of including multistep processes involving inelastic excitation in the targets and residual nuclei as noted above were not expected to be significant because of the relatively small deformation para-

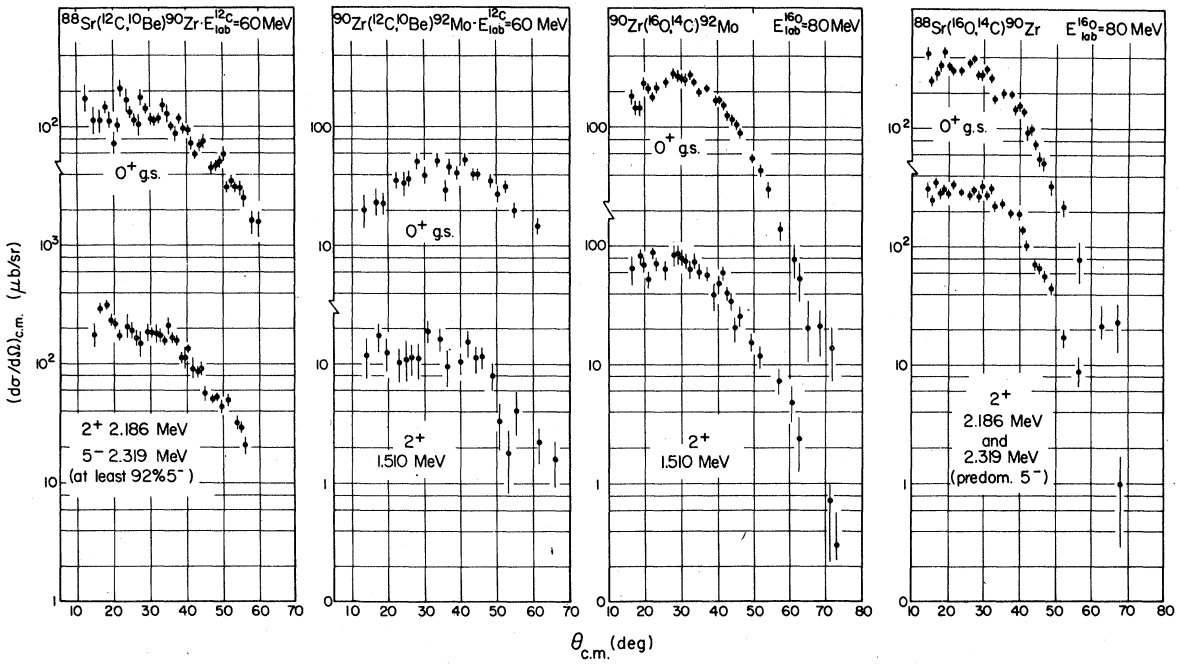

FIG. 2. Angular distributions for the (^{16}O, ^{14}C) and (^{12}C, ^{10}Be) reactions, measured at 80 and 60 MeV incident beam energies, respectively, on ^{88}Sr and ^{90}Zr.

meters involved.[24-26] In fact, the inclusion in our reaction model of inelastic excitation to the 2^+ state in the target and the residual nucleus for the reaction ^{90}Zr(^{16}O, ^{14}C)^{92}Mo, for example, produced a 40% increase in the magnitude of the predicted cross section to the 2^+ state of the residual nucleus as compared with predictions involving only direct amplitudes, but led to closely similar angular distribution shapes. This change of absolute predicted magnitude could still be considered small in view of the fact that the pure sequential process in general was found to contribute a cross section about five times larger than that for the pure direct process, for the reactions in the present study. The additional multistep processes involving inelastic excitation of the projectiles were not investigated. In the (^{16}O, ^{14}C) reactions, the large excitation energies involved in such processes tend to diminish their importance, and in any event the inclusion of inelastic excitations in the coupled channel codes could have greatly complicated our analyses. In the present study, attention is focused on the contributions from pure direct, pure sequential, and the coherent sum of these two processes.

The bound-state wave functions were generated with a potential which included a Woods-Saxon shape nuclear potential, a spin-orbit potential of standard form, and a Coulomb potential. The depth of the Woods-Saxon potential was varied so as to bind the transferred nucleon at the measured separation energy. In calculating the contribution of the two-proton direct (simultaneous) transfer process to the final cross section, each of the transferred protons was assumed to be bound at one-half the measured two-proton separation energy while in each step of a sequential transfer, the appropriate measured one-proton separation energies were used. The Coulomb interaction term was neglected in constructing the form factors. It has been reported[27] that although neglecting the Coulomb interaction can introduce a 30% difference in cross-section magnitudes for the type of reactions studied in this work, generally the differences in predicted shapes are found to be quite small.

The form factor for the direct transfer process was calculated by expanding the two-nucleon overlap as a multipole series in the relative and center-of-mass angular momenta of the transferred nucleons; this series was found to converge rapidly for the population of 0^+ states in Ref. 34, and for 2^+ states in the present work. Consequently, in calculating the contribution to the final cross section from the direct process, the relative orbital angular momentum was truncated at a value of $3\hbar$, as required for form factor convergence. For the calculations of the direct transfer 70 partial waves were included, while for the sequential transfer 65 partial waves were included: The S-matrix elements were found to converge at these values.

In the following analyses, we have used the trun-

TABLE I. Spectroscopic amplitudes for one- and two-nucleon transfers in the target-residual nucleus system ("heavy system") within the truncated $(2p_{1/2}, 1g_{9/2})$ shell model.

Two-proton transfer spectroscopic amplitudes for heavy systems [a]

	$(2p_{1/2})^2$	$(1g_{9/2})^2$	$(2p_{1/2})(1g_{9/2})$
$^{88}Sr(0^+) \rightarrow {}^{90}Zr(0_1^+)$	0.8147	−0.5799	0.0
$^{88}Sr(0^+) \rightarrow {}^{90}Zr(0_2^+)$	0.5799	+0.8147	0.0
$^{88}Sr(0^+) \rightarrow {}^{90}Zr(2^+)$	0.0	1.0	0.0
$^{88}Sr(0^+) \rightarrow {}^{90}Zr(5^-)$	0.0	0.0	1.0
$^{90}Zr(0^+) \rightarrow {}^{92}Mo(0^+)$	−0.4843	1.084	0.0
$^{90}Zr(0^+) \rightarrow {}^{92}Mo(2^+)$	0.0	0.9300	

One-proton transfer spectroscopic amplitudes for heavy systems

$^{88}Sr(0^+) \rightarrow {}^{89}Y(\frac{1}{2}^-)$	−0.9487 [b]
$^{88}Sr(0^+) \rightarrow {}^{89}Y(\frac{9}{2}^+)$	+0.9380 [b]
$^{89}Y(\frac{1}{2}^-) \rightarrow {}^{90}Zr(0^+)$	+1.1521 [c]
$^{89}Y(\frac{9}{2}^+) \rightarrow {}^{90}Zr(0^+)$	+0.8124 [c]
$^{90}Zr(0^+) \rightarrow {}^{91}Nb(\frac{9}{2}^+)$	+0.9657 [a]
$^{90}Zr(0^+) \rightarrow {}^{91}Nb(\frac{1}{2}^-)$	−0.5799 [a]
$^{91}Nb(\frac{9}{2}^+) \rightarrow {}^{92}Mo(0^+)$	+1.5834 [a]
$^{91}Nb(\frac{9}{2}^+) \rightarrow {}^{92}Mo(2^+)$	+1.3642 [a]
$^{91}Nb(\frac{1}{2}^-) \rightarrow {}^{92}Mo(0^+)$	+1.1809 [a]

[a] From Ref. 29.
[b] From Ref. 30.
[c] From Ref. 29 and sum rules.

cated $(2p_{1/2}, 1g_{9/2})$ shell model which has successfully reproduced many experimental data on nuclear structure in the mass-90 region,[11-17] to describe the structure of the targets and residual nuclei. As an additional check on this adequacy we examined the population of the two lowest 0^+ states in ^{90}Zr. Within the framework of this truncation these states have the wave functions[29]

$$\psi_0 = 0.8147(p_{1/2})^2 - 0.5799(g_{9/2})^2 ,$$

$$\psi_1 = 0.5799(p_{1/2})^2 + 0.8147(g_{9/2})^2 .$$

Inserting these wave functions into our reaction model we predict ratios of 70 and 80 for ground to excited states for the reactions $^{88}Sr(^{12}C, ^{10}Be)^{90}Zr$ and $^{88}Sr(^{16}O, ^{14}C)^{90}Zr$. Experimentally we have established lower limits of 75 and 50 for this ratio and the model reproduction of this large ratio gives us additional confidence in its adequacy in this mass region.

The spectroscopic amplitudes—as defined by French[28]—for one- and two-nucleon transfer in the target-residual nucleus system (the "heavy" system) within the truncated $(2p_{1/2}, 1g_{9/2})$ shell model calculated by Brown, Chung and King[29] are listed in Table I; those for the projectile-reaction product system (the "light" system) calculated from the coefficients of fractional parentage given by Cohen and Kurath[31,32] are listed in Table II.

TABLE II. Spectroscopic amplitudes for the projectile-reaction product system ("light system") calculated from the coefficients of fractional parentage.

Two-proton transfer spectroscopic amplitudes S for light systems [a]

	$(1p_{3/2})^2$	$(1p_{1/2})^2$
$^{12}C(0^+) \rightarrow {}^{10}Be(0^+)$	+0.874	+0.486
$^{16}O(0^+) \rightarrow {}^{14}C(0^+)$	+0.405	+0.914

One-proton transfer spectroscopic amplitudes S for light systems [b]

$^{12}C(0^+) \rightarrow {}^{11}B(\frac{3}{2}^-)$	−1.6880
$^{12}C(0^+) \rightarrow {}^{11}B(\frac{1}{2}^-)$	+0.8678
$^{11}B(\frac{3}{2}^-) \rightarrow {}^{10}Be(0^+)$	−0.6557
$^{11}B(\frac{1}{2}^-) \rightarrow {}^{10}Be(0^+)$	+0.7649
$^{16}O(0^+) \rightarrow {}^{15}N(\frac{1}{2}^-)$	+1.4142 [c]
$^{16}O(0^+) \rightarrow {}^{15}N(\frac{3}{2}^-)$	+2.0000 [c]
$^{15}N(\frac{1}{2}^-) \rightarrow {}^{14}C(0^+)$	+0.9141
$^{15}N(\frac{3}{2}^-) \rightarrow {}^{14}C(0^+)$	+0.2867

[a] From Ref. 32 [Cohen + Kurath coefficients of fractional parentage (CFP)] and $S = -[N(N-1)/2]^{1/2} C^{T' T \Delta T}_{T_z' T_z - T_z} \times (\mathrm{CFP})_{\mathrm{Cohen+Kurath}}$. Also, note that in our definition, there is a sign difference from the CFP's calculated in Ref. 32.
[b] From Ref. 31 and $S = \sqrt{N} C^{T' T \Delta T}_{T_z' T_z - T_z} (\mathrm{CFP})_{\mathrm{Cohen+Kurath}}$.
[c] From Ref. 31 and sum rules.

The optical model parameters used in the analyses of the transfer reaction data were based on those obtained by fitting the elastic data. The results of the parameter search are compared with the measured elastic scattering in Fig. 3, and are given as potential set I in Table III.

A. Configuration dependence of direct transfer processes in no-recoil and in full-recoil DWBA models

In order to investigate the possible importance of including recoil effects, full-recoil calculations were first carried out separately for the $(p_{1/2})^2$ and $(g_{9/2})^2$ configurations leading to the ground state of ^{92}Mo in the $^{90}Zr(^{16}O, ^{14}C)^{92}Mo$ reaction. Figure 4 shows a comparison of the no-recoil with the full-recoil results. The ratio of calculated cross sec-

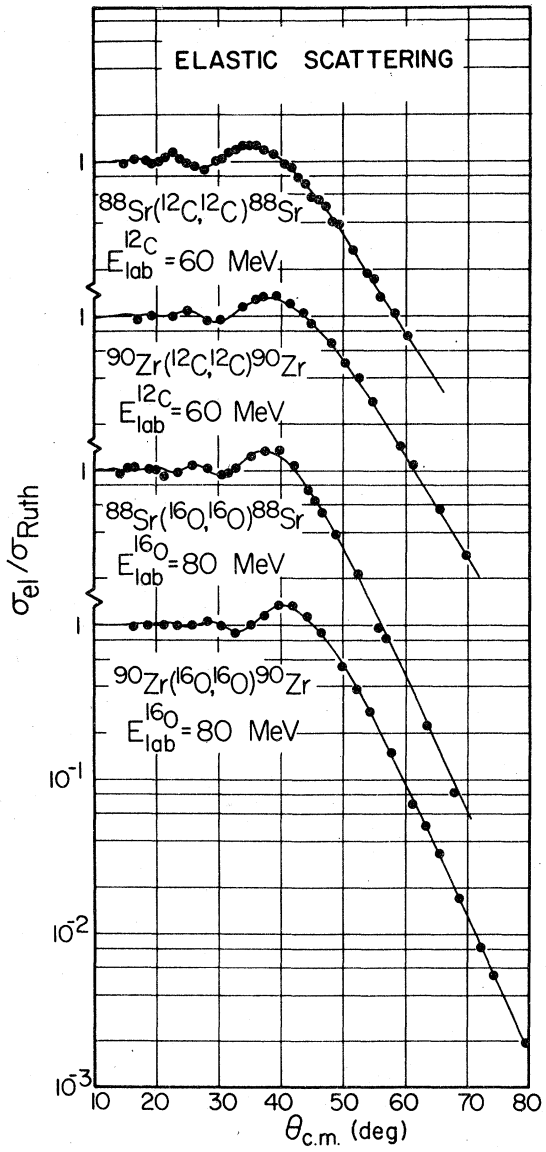

FIG. 3. Measured elastic scattering angular distributions. The solid lines are the results of optical model calculations using potential set I (Table III).

tions for the pure $(2p_{1/2})^2$ configuration to that for the pure $(1g_{9/2})^2$ configuration is ~2.5 in the no-recoil approximation and ~1.0 in the full-recoil treatment. The relative *calculated* cross section for the population of different states in the residual nucleus can thus be changed substantially by including recoil properly when mixing among limited structural configurations is involved; this configuration dependence of two-nucleon direct transfer processes in no-recoil and full-recoil DWBA models has not been emphasized previously. In addition to this observation, the full-recoil calculations were found to predict a more forward-peaked angular distribution and a much smaller absolute cross section for *either* configuration, as compared with those from no-recoil calculations (Fig. 4). This result is similar to that of Bayman for the case of the ^{62}Ni(^{18}O,^{16}O)^{64}Ni$_{g.s.}$ reaction at E_{lab} = 65 MeV (Ref. 33) in the sense that he found that the full-recoil calculation predicted a cross section five times smaller than did the no-recoil. Our results contrast, however, with the calculation of Takemasa for the reaction ^{12}C(^{18}O,^{16}O)^{14}C$_{g.s.}$ at E_{lab} = 24 MeV,[34] in which neither the cross-section magnitudes nor the angular distribution shapes were modified significantly by inclusion of full recoil except for minor shape changes at forward angles.

The configuration-dependent recoil effects found in our test calculations mandated that the present calculations be carried out in full recoil, at the cost of substantially greater computer time. As a matter of possible interest, a typical angular distribution calculation in full recoil including both direct and sequential contributions required 1–2 hours of CDC 6600 CPU time. It should be noted, however, that this time estimate is considerably inflated because a somewhat inefficient calculational sequence was employed to facilitate comparisons of contributions arising from different configurations.

B. Sequential effects in the reaction ^{90}Zr(^{16}O, ^{14}C)^{92}Mo

As a preliminary to the sequential analysis, the *one*-proton reaction, ^{90}Zr(^{16}O,^{15}N)^{91}Nb, was subjected to detailed study. The experimental data are shown in Fig. 5, together with the result of DWBA analyses of this one-proton transfer reaction. A minor modification (2% increase in real radius) in the optical potential which fits the elastic data was required to bring the predicted angular distribution into agreement with the experimental transfer data. All the calculations for the *two*-proton transfer reaction, ^{90}Zr(^{16}O,^{14}C)^{92}Mo, presented hereafter were carried out with this modified, or one-proton transfer, potential in the entrance, intermediate, and exit channels. In the truncated $(2p_{1/2}, 1g_{9/2})$ shell model used, two intermediate channels, populating the $\frac{9}{2}^+$ ground and the $\frac{1}{2}^-$ first excited states in ^{91}Nb, are considered for the sequential processes, as shown in Fig. 6. A comparison of the predicted shapes of the angular distributions for pure two-step sequential processes with those for pure direct processes is shown in Fig. 7(a) for each configuration. It is evident that for this reaction there are predicted differences at forward angles. Especially for the contribution of the $(2p_{1/2})^2$ configuration to the ^{92}Mo ground-state transition, the sequential model pre-

TABLE III. Optical parameters used in the analyses.

Reaction	Parameter set [a]	V (MeV)	W (MeV)	r_{0r} (fm)	r_{0i} (fm)	a_r (fm)	a_i (fm)	r_c (fm)
^{88}Sr(^{16}O, ^{14}C)^{90}Zr	I	100.0	30.0	1.1947	1.1947	0.5274	0.5274	1.2
	II			1.2724				
^{90}Zr(^{16}O, ^{14}C)^{92}Mo	I	100.0	30.0	1.2044	1.2044	0.5155	0.5155	1.2
	II			1.3068				
	III			1.2285				
^{88}Sr(^{12}C, ^{10}Be)^{90}Zr	I	100.0	30.0	1.2036	1.2036	0.4805	0.4805	1.2
	II			1.3000				
^{90}Zr(^{12}C, ^{10}Be)^{92}Mo	I	100.0	30.0	1.1718	1.1718	0.5297	0.5297	1.2

[a] Parameter set I: elastic potential. Parameter set II: potential which is needed to fit the general shape of transfer reaction in full-recoil analyses. Parameter set III: one-proton potential.

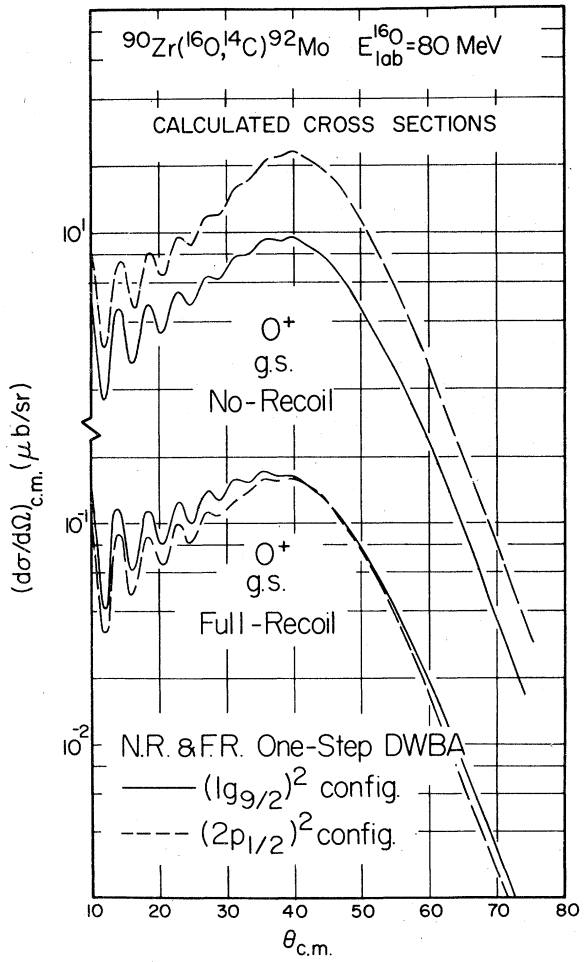

FIG. 4. Comparison of full-recoil and no-recoil calculations for the ^{90}Zr(^{16}O, ^{14}C)^{92}Mo ground-state reaction. The curves show the results of direct, one-step calculations involving the $(1g_{9/2})^2$ proton configuration only (solid lines) and the $(2p_{1/2})^2$ configuration only (broken lines).

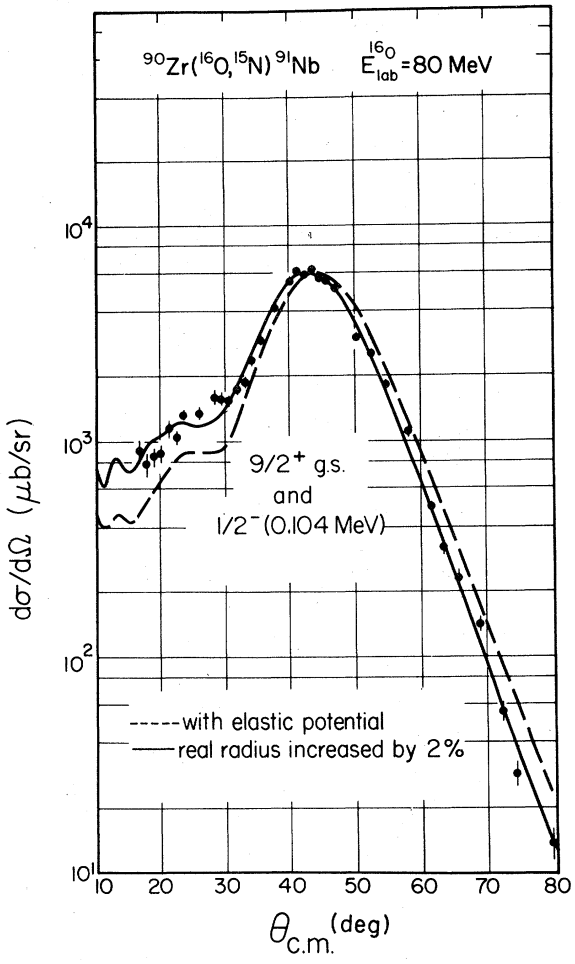

FIG. 5. Measured and calculated (full-recoil DWBA) angular distributions for the ^{90}Zr(^{16}O, ^{15}N)^{91}Nb reaction. The optical potential which fits the entrance channel elastic scattering (set I, Table III) was used to calculate the broken curve, while an improved result (solid curve) was obtained by increasing the real radius of the optical potential by 2%. The corresponding parameters are given as set III in Table III.

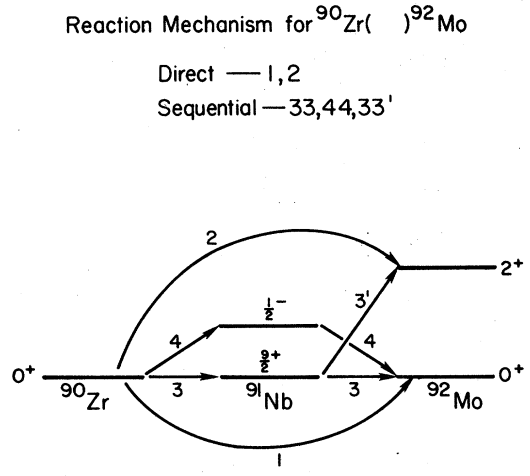

FIG. 6. Transfer routes included in the sequential two-proton-transfer calculations for reactions on a ^{90}Zr target.

dicts a much more forward-peaked angular distribution than is obtained in direct transfer, and provides improved agreement with the experimental data. This difference is, however, small for the contribution of the $(g_{9/2})^2$ configuration.

Qualitatively, this difference can be understood in terms of the relative magnitudes of the $2p_{1/2}$ and $1g_{9/2}$ radial wave functions in the surface regions of importance in these transfer reactions. The form factor for sequential $2p_{1/2}$ transfer falls off faster in r space than does that for the corresponding direct process, producing stronger localization in configuration, and therefore in orbital angular momentum space. Since the calculated full-recoil radial form factors are two dimensional, it is not easy to illustrate this comparison; however, the effect can be observed in the S-matrix elements for the various processes. In Fig. 8(a) we show that the width of the calculated S-matrix element distribution in L space is in general narrower for the sequential processes, which is reflected in a wider angular spread, i.e., a more forward-peaked angular distribution. This difference in the width of the S-matrix element is larger for the $(p_{1/2})^2$ configuration, which explains the enhanced forward angle calculations for that configuration.

The extent to which inclusion of sequential amplitudes can alter the shape of the predicted angular distribution to the 0$^+$ ground state in the residual nucleus depends on (1) the relative magnitude of the calculated cross sections for sequential and direct transfer, and (2) the relative magnitude of the calculated cross sections for different configura-

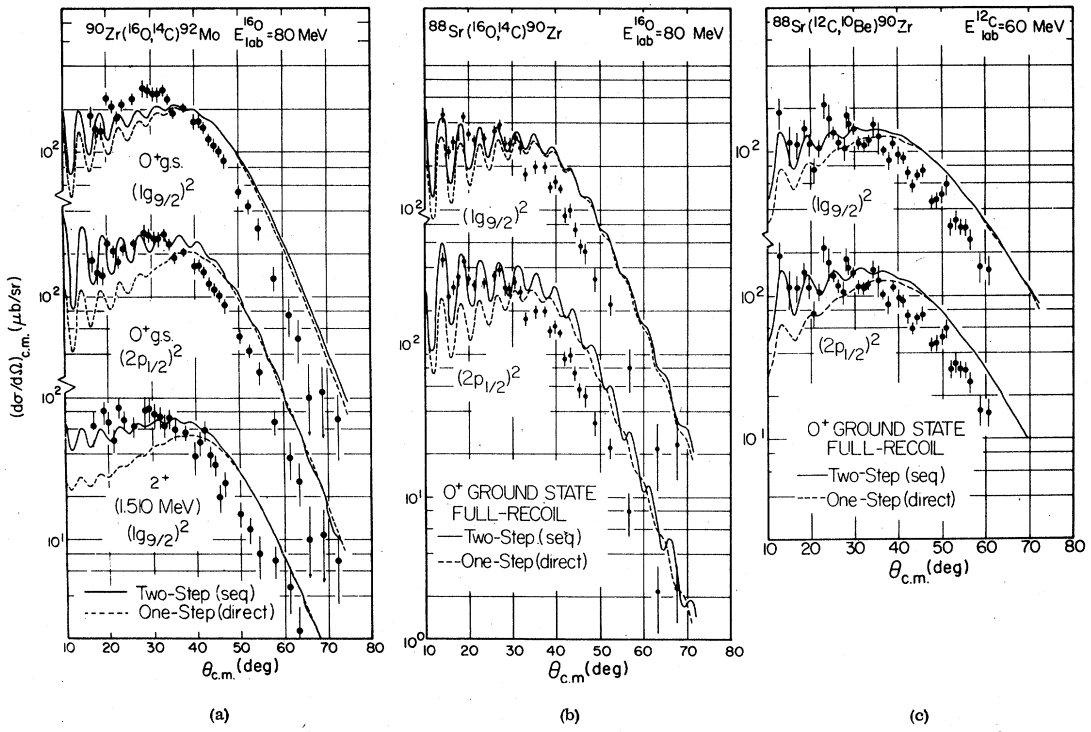

FIG. 7. Comparison of sequential and direct calculations for transfer in the pure $(1g_{9/2})^2$ and $(2p_{1/2})^2$ configurations. The measured angular distributions are also shown. The three panels refer to (a) ^{90}Zr(^{16}O, ^{14}C)^{92}Mo, (b) ^{88}Sr(^{16}O, ^{14}C)^{90}Zr, and (c) ^{88}Sr(^{12}C, ^{10}Be)^{90}Zr. The calculated curves are arbitrarily normalized to one another at backward angles for display purposes.

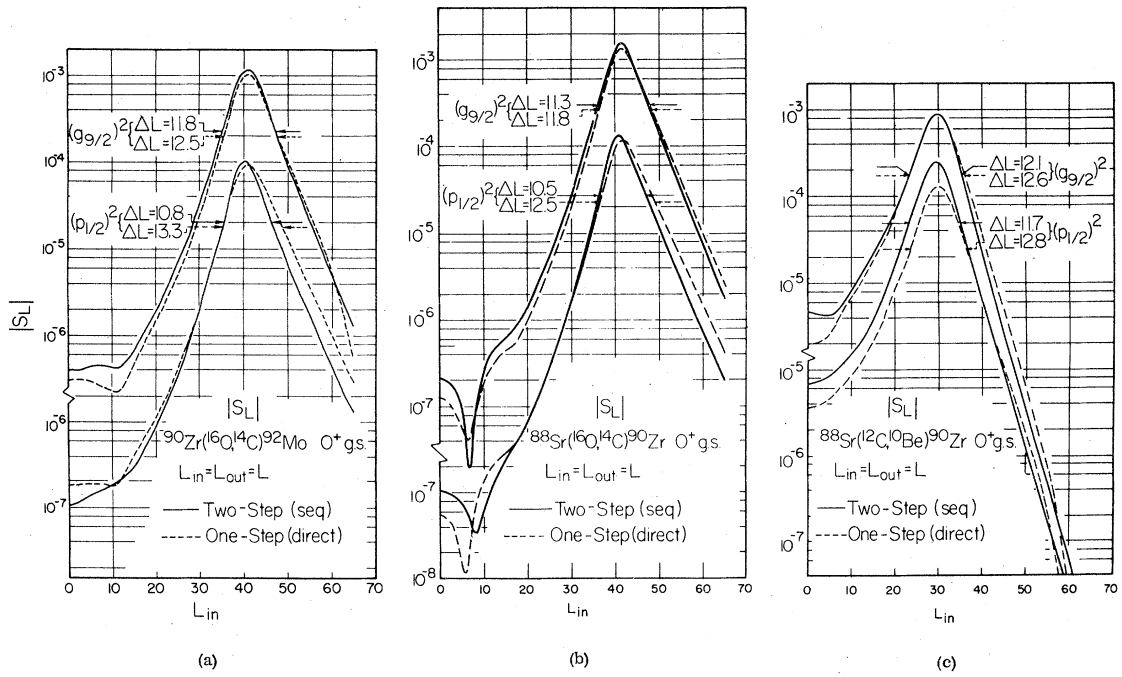

FIG. 8. Comparison of diagonal S-matrix-element magnitudes for sequential and direct ground-state transfer calculations involving pure $(1g_{9/2})^2$ and $(2p_{1/2})^2$ configurations. The three panels refer to (a) ^{90}Zr(^{16}O, ^{14}C)^{92}Mo, (b) ^{88}Sr(^{16}O, ^{14}C)^{90}Zr, and (c) ^{88}Sr(^{12}C, ^{10}Be)^{90}Zr.

tions. The calculated sequential transfer process contributes, as shown in Fig. 9(a), 4 times the cross section to the ground state and eight times that to the 2^+ state, as compared with the direct process. Consequently the sequential transfer process is the dominant one in determining the shape and magnitude of the cross section. In Fig. 10(a), we show that the $(2p_{1/2})^2$ contribution to the calculated ground-state cross section is much smaller than the $(1g_{9/2})^2$ contribution, reflecting the much smaller spectroscopic amplitudes for the former. As a result, the coherently summed calculated cross sections of the two configurations for the ground-state transitions, as shown in Fig. 9(a) for various processes, have shapes more similar to those of the pure $(g_{9/2})^2$ configuration. The difference between the "sequential+direct" and the "direct" angular distributions is not as large as might have been expected in cases where $(p_{1/2})^2$ rather than $(g_{9/2})^2$ is the main configuration. Examples of the latter situation will be discussed in Sec. III C.

The solid curves in Fig. 9 show the angular distributions resulting from the combined direct-plus-sequential calculations. While the calculated angular distribution shapes are much improved with the inclusion of sequential transfer, significant discrepancies remain. Better fits *can* be obtained using modified optical potentials (see, e.g., Fig. 11) without changing the quantitative conclusions in any significant manner, but as these modifications lack theoretical justification we continue the discussion in terms of the potential which fits the one-nucleon transfer data.

All calculations reproduced the relative population of the 2^+ and 0^+ states to within a factor of roughly 2. The population of the 2^+ state was overestimated, as compared with that of the 0^+ ground state, by ~10% in a one-step direct DWBA, by a factor of ~2.5 in the sequential process, and by a factor of 2.1 in the coherent sum of the two processes. This factor of ~2 persisted when the optical model parameters were changed, as in Fig. 11. The absolute normalization factors required to obtain the best fits to the experimental absolute cross sections are given in Table IV. Although the direct transfer mechanism provided the best reproduction of the *relative* magnitude, it only contributed a small fraction of the final cross-section prediction. The predicted *absolute* magnitudes of the cross sections were increased by a factor of 5, ~8 by including the sequential transfer process, but the absolute cross sections were still underestimated (Table IV). This discrepancy between theoretical and experimental cross sections is common to many reaction calculations,[35] and may arise from inadequacies of the potential used in generating the bound-state wave functions in the light (pro-

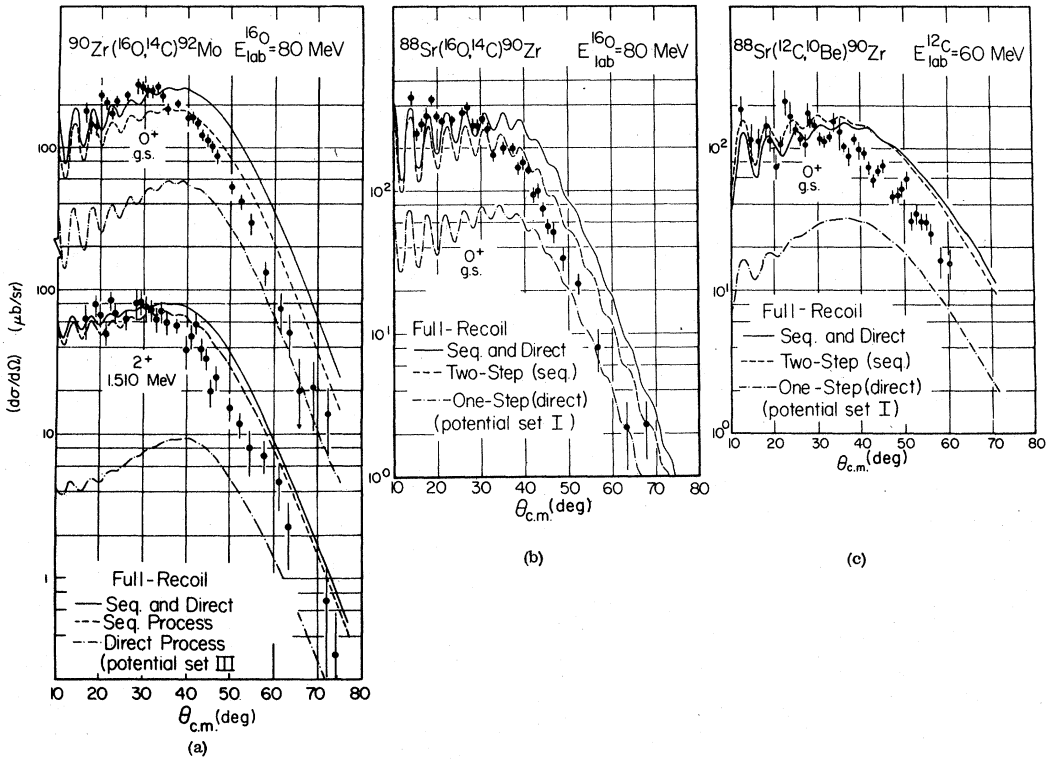

FIG. 9. Calculated direct and sequential contributions to the reactions (a) ^{90}Zr(^{16}O, ^{14}C)^{92}Mo, (b) ^{88}Sr(^{16}O, ^{14}C)^{90}Zr, and (c) ^{88}Sr(^{12}C, ^{10}Be)^{90}Zr. The calculations are normalized to the data shown by the factors given in column 4 of Table IV. The wave-function amplitudes given in Tables I and II were used in the calculations.

jectile-reaction product) and heavy (target-residual nucleus) systems or from the inadequacy of the size of the configuration space used in describing the light or heavy system overlaps. These possibilities, because of the magnitude of the required calculational effort, have not been explored extensively in the present analyses.

The sensitivity of the pure sequential process to the intermediate Q value (the Q value of the first-step transition) is illustrated in Fig. 12. Here the binding energies used to generate the form factors in the heavy systems were changed in the entrance and exit channels while preserving the overall Q value for the two-nucleon transfer. It follows from Fig. 12 that there can be small intermediate-Q-dependent differences in the shapes of the sequential angular distributions at forward angles and rather large changes in the magnitudes of the calculated cross sections. The Q value for the first- and second-step transitions Q_1 and Q_2 were rather arbitrarily chosen as $Q_1 = Q_2 = -4.86$ MeV; this does not result in substantial differences in the calculated cross sections as compared with those with experimental Q values ($Q_1 = -6.69$ MeV). The set $Q_1 = -1.34$ MeV and $Q_2 = -8.37$ MeV was chosen so that the second-step transition has a well-matched Q value, and resulted in a substantial increase in the magnitude of the cross sections and a less forward-peaked shape in angular distribution for the 0$^+$ ground state. This suggests that it may also be possible to distinguish experimentally between direct and sequential processes if the situation is carefully chosen with favorable nuclear structure and intermediate Q values.

C. The reactions ^{88}Sr(^{16}O, ^{14}C)^{90}Zr and ^{88}Sr(^{12}C, ^{10}Be)^{90}Zr

The calculated cross sections for population of the 0$^+$ ground states in the respective residual nuclei in the ^{88}Sr(^{16}O, ^{14}C)^{90}Zr and ^{88}Sr(^{12}C, ^{10}Be)^{90}Zr reactions are shown in Figs. 7(b) and 7(c). The sequential processes with formation of ^{89}Y in its $\frac{1}{2}^-$ ground and $\frac{9}{2}^+$ first excited states are considered as intermediate channels. Similar to the situation encountered in the reaction ^{90}Zr(^{16}O, ^{14}C)^{92}Mo, the difference in the shapes of the calculated angular distributions for direct and sequential processes at forward angles is larger for the $(p_{1/2})^2$ configuration; this again follows from the localization of the S-matrix elements in L space, as shown in Figs. 8(b) and 8(c). In contrast to the situation in the reaction ^{90}Zr(^{16}O, ^{14}C)^{92}Mo, however, where the $(g_{9/2})^2$ configuration contributes in a major fashion

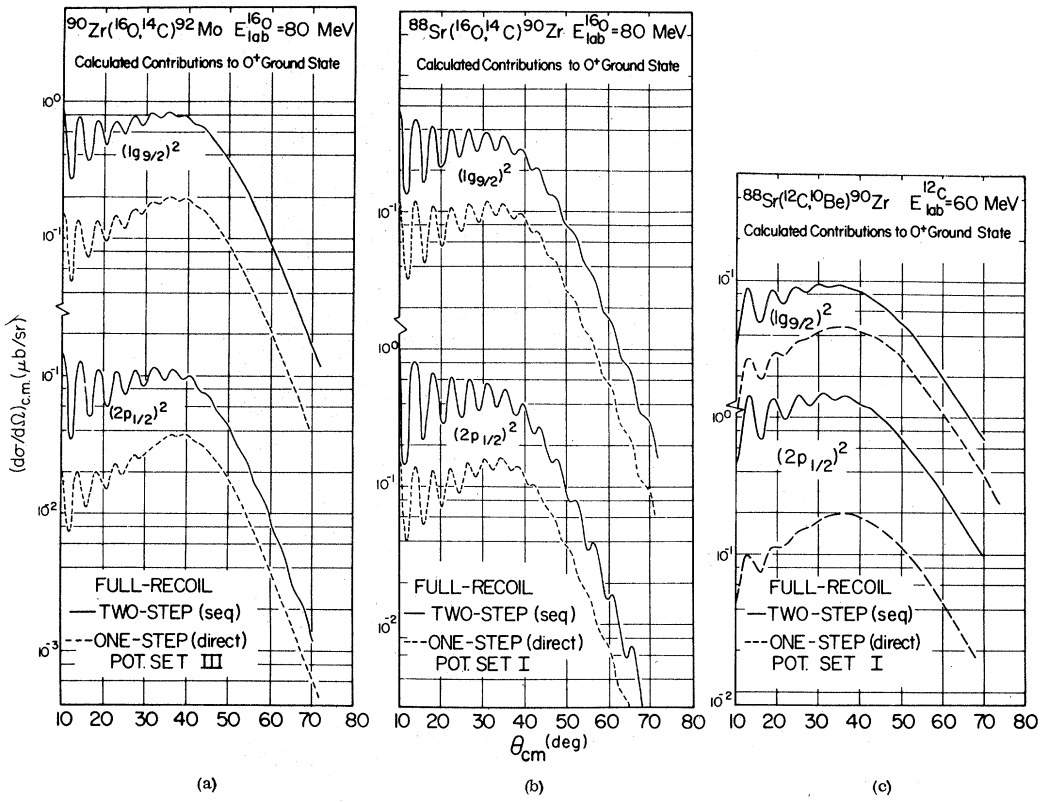

FIG. 10. Comparison of calculated direct and sequential contributions (for pure heavy-particle wave-function configurations) to the reactions (a) $^{90}Zr(^{16}O,^{14}C)^{92}Mo$, (b) $^{88}Sr(^{16}O,^{14}C)^{90}Zr$, and (c) $^{88}Zr(^{12}C,^{10}Be)^{90}Zr$. The wave-function amplitudes given in Tables I and II were used.

to the overlap integral in the heavy system, in the $^{88}Sr(^{16}O,^{14}C)^{90}Zr$ and $^{88}Sr(^{12}C,^{10}Be)^{90}Zr$ reactions the dominant configuration is $(p_{1/2})^2$; this is reflected, as shown in Figs. 10(b) and 10(c), in a larger relative contribution to the total cross section from the $(p_{1/2})^2$ configuration. The sequential process contributes a cross section three times larger than the direct for the reaction $^{88}Sr(^{16}O,^{14}C)^{90}Zr$ and 5 times larger for the reaction $^{88}Sr(^{12}C,^{10}Be)^{90}Zr$.

It should be noted that, as can be deduced from Fig. 9, the direct and sequential processes to the 0^+ ground state in the residual nuclei interfere constructively for the reactions $^{88}Sr(^{16}O,^{14}C)^{90}Zr$ and $^{90}Zr(^{16}O,^{14}C)^{92}Mo$, and destructively for the reaction $^{88}Sr(^{12}C,^{10}Be)^{90}Zr$. It was found in the calculations that sequential transfer in the $(1p_{1/2})^2$ configuration in the light (projectile-reaction product) systems interferes constructively with the direct process, while that from the $(1p_{3/2})^2$ configuration in the light system interferes destructively with the direct process. The contribution from the $(1p_{3/2})^2$ configuration for the reaction $^{88}Sr(^{12}C,^{10}Be)$ ^{90}Zr, however, is much larger than that from the $(1p_{1/2})^2$ configuration, and therefore the net amplitude from sequential process interferes destructively with that from the direct process.

Similar calculations for the $2^+, 5^-$ angular distribution (predominantly 5^-) could not be carried out in detail because of limitations inherent in the DOE/NYU CDC-6600 computer system in use. These involve round-off errors for a full-recoil calculation including adequately high angular momentum transfer and allowing up to three units of relative orbital angular momentum for the nucleons transferred.

The transfer data from the reaction $^{90}Zr(^{12}C,$ $^{10}Be)^{92}Mo$ presented in Fig. 2 were not subjected to full-recoil analysis because the general trends observed in the experimental data of the four reactions including $^{90}Zr(^{12}C,^{10}Be)^{92}Mo$ may be explained by the Q value and projectile/target dependence summarized in the following section, and the considerable effort required to do so would not add significantly to our understanding of the systematics of reaction behavior in this mass region.

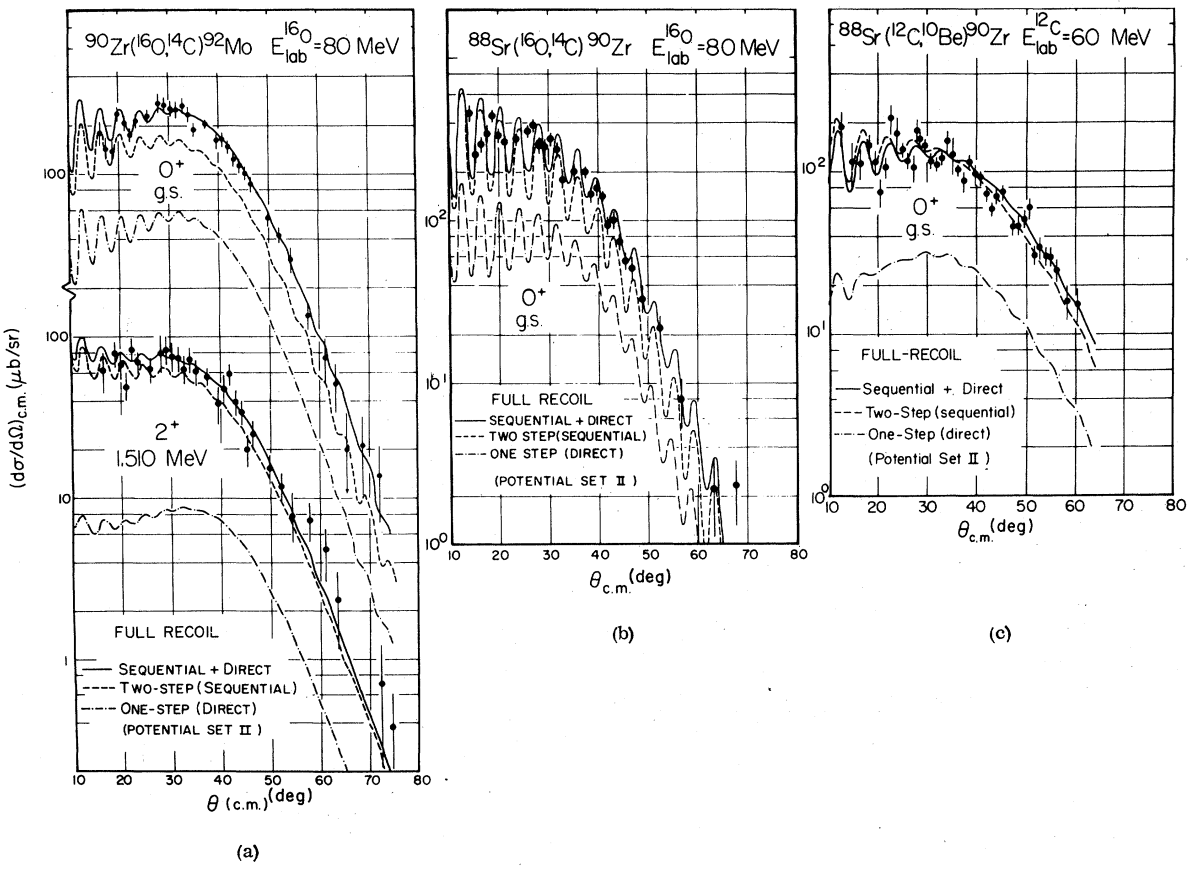

FIG. 11. Calculations similar to those of Fig. 9, except that modified optical potentials (2% increase in real radius—parameter sets II in Table III) were used.

D. Comparison of the reactions $^{88}Sr(^{16}O, ^{14}C)^{90}Zr$, $^{90}Zr(^{16}O, ^{14}C)^{92}Mo$, $^{88}Sr(^{12}C, ^{10}Be)^{90}Zr$, and $^{90}Zr(^{12}C, ^{10}Be)^{92}Mo$

Q value and projectile/target dependence: Systematic trends in the experimentally observed angular distributions for the population of 0^+ ground states in the respective residual nuclei in the reactions $^{88}Sr(^{16}O, ^{14}C)^{90}Zr$, $^{90}Zr(^{16}O, ^{14}C)^{90}Mo$, $^{88}Sr(^{12}C, ^{10}Be)^{90}Zr$, and $^{90}Zr(^{12}C, ^{10}Be)^{92}Mo$ are shown in Fig. 13; here we have drawn only smooth curves through the data points to highlight the trends.

We first consider the absolute magnitudes of the cross sections. The reaction $^{90}Zr(^{12}C, ^{10}Be)^{92}Mo$ stands out as having a much smaller cross section as compared to all the others. It may be noted in Table V that this reaction has the best matched Q value for a direct transfer process; however, these matching conditions are not as important to the final cross sections as are those for the corresponding sequential transfer process which, as discussed above, dominates the transfer process. Indeed, although none of the transitions are perfectly matched in their Q values, *one* of the two steps in the sequential transfer was closely matched in Q value in each reaction *except* $^{90}Zr(^{12}C, ^{10}Be)^{92}Mo$; both the first- and second-step transitions of the

TABLE IV. Normalization factors $N = \sigma_{exp}/\sigma_{theo}$ for full-recoil analyses.

Reactions	State in residual nucleus	Direct	Sequential	Direct + sequential	Potential parameter set (Table V-4)
$^{88}Sr(^{16}O, ^{14}C)^{90}Zr$	0^+	650	185	143	I
$^{90}Zr(^{16}O, ^{14}C)^{92}Mo$	0^+	631	190	139	III
	2^+	574	74	65	III
$^{88}Sr(^{12}C, ^{10}Be)^{90}Zr$	0^+	345	64	70	I

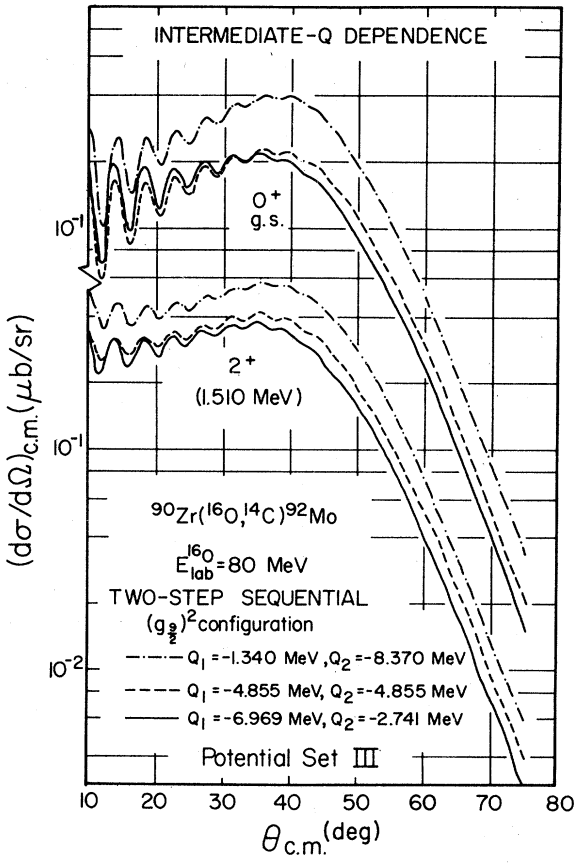

FIG. 12. Calculated dependence of sequential contributions to the $^{90}Zr(^{16}O, ^{14}C)^{92}Mo$ reactions on intermediate Q value, as discussed in the text.

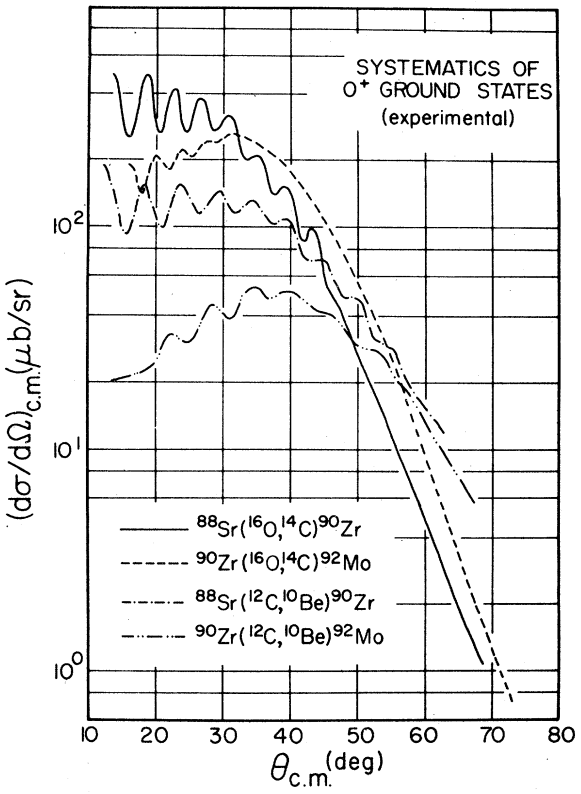

FIG. 13. Comparison of ground-state angular distributions for the four reactions studied. The curves shown were simply drawn to pass through the data points.

sequential transfer process in this reaction are mismatched in Q value by at least 3 MeV. This reaction also has the worst L-matching conditions for the two transitions comprising the sequential transfer. The facts that the reaction $^{90}Zr(^{12}C, ^{10}Be)^{92}Mo$ has the most unfavorable L- and Q-matching conditions for sequential transfer and that sequential transfer amplitudes were found to be dominant in this mass region are consistent with the experimental observation that its cross sections are

TABLE V. Reaction systematics.

Reaction	Laboratory bombarding energy (MeV)	Classical grazing angle	Ground state Q value (MeV)	Optimum Q value (MeV)	Favored L transfer ($E_{ex}=0.0$) ($\hbar$)	Half two-proton/proton separation energies Light system (MeV)	Heavy system (MeV)
$^{88}Sr(^{16}O, ^{14}C)^{90}Zr$	80.0	40.7°	−6.902	−14.251	1.12	11.168	7.716
$^{90}Zr(^{16}O, ^{14}C)^{92}Mo$	80.0	42.3°	−9.710	−14.434	2.79	11.168	6.312
$^{88}Sr(^{12}C, ^{10}Be)^{90}Zr$	60.0	40.5°	−11.754	−15.747	4.23	13.594	7.716
$^{90}Zr(^{12}C, ^{10}Be)^{92}Mo$	60.0	42.1°	−14.563	−15.563	6.11	13.594	6.312
$^{88}Sr(^{16}O, ^{15}N)^{89}Y$	80.0		−5.061	−6.903	1.90	12.128	7.067
$^{89}Y(^{15}N, ^{14}C)^{90}Zr$	(73.187)		−1.841	−7.571	−0.78	10.207	8.366
$^{90}Zr(^{16}O, ^{15}N)^{91}Nb$	80.0		−6.969	−7.005	3.33	12.128	5.159
$^{91}Nb(^{15}N, ^{14}C)^{92}Mo$	(71.003)		−2.741	−7.433	−0.54	10.207	7.466
$^{88}Sr(^{12}C, ^{11}B)^{89}Y$	60.0		−8.890	−7.642	4.70	15.957	7.067
$^{89}Y(^{11}B, ^{10}Be)^{90}Zr$	(49.337)		−2.863	−7.881	−0.47	11.229	8.366
$^{90}Zr(^{12}C, ^{11}B)^{91}Nb$	60.0		−10.800	−7.721	6.38	15.957	5.159
$^{91}Nb(^{11}B, ^{10}Be)^{92}Mo$	(47.235)		−3.763	−7.606	−0.27	11.229	7.066

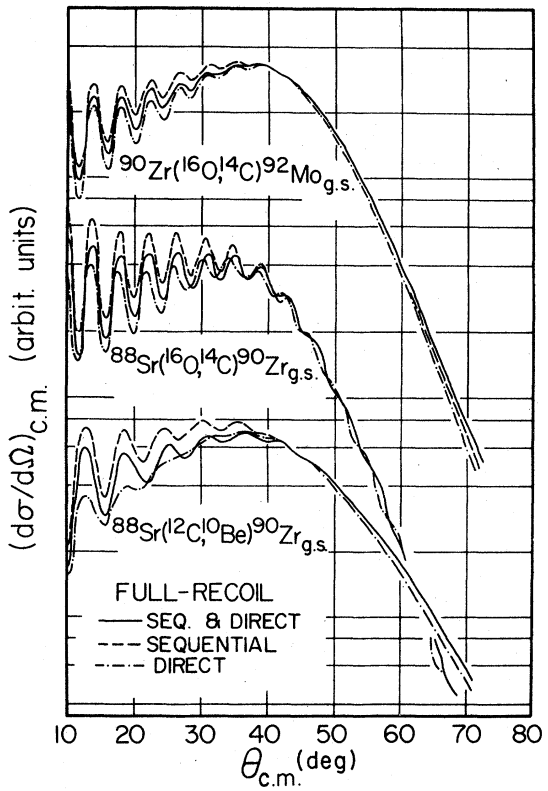

FIG. 14. Summary of calculated dependencies of angular distribution shapes on reaction mechanism. The three curves for each reaction are arbitrarily normalized at the grazing angle to facilitate the shape comparison.

much lower than those from the other three reactions studied.

We then examine the shapes of the angular distributions in Fig. 13. It may be seen that the reactions induced by ^{12}C and ^{16}O projectiles lead to characteristically different angular distribution shapes, with the former yields less strongly localized in angle. This projectile dependence, which is adequately reproduced in the calculations, results primarily from the differences in the two-proton binding energies in the ^{12}C and ^{16}O systems. The larger binding energies in the former produce form factors which are more strongly localized in both configuration and angular momentum space, and hence result in wider angular distributions for the $(^{12}C,^{10}Be)$ reactions.

Figure 14 shows a comparison of predicted angular distribution shapes of the residual ground states in the reactions $^{90}Zr(^{16}O,^{14}C)^{92}Mo$, $^{88}Sr(^{16}O,^{14}C)^{90}Zr$, and $^{88}Sr(^{12}C,^{10}Be)^{90}Zr$ for pure direct, pure sequential, and the coherent sum of these processes. It is evident that including the sequential transfer process does not introduce dramatic changes in the shape of the angular distribution; however, it does introduce some difference at forward angles. This difference is observed in the calculations to be larger for the reactions $^{88}Sr(X, Y)^{90}Zr$ than for the reaction $^{90}Zr(^{16}O,^{14}C)^{90}Mo$. It may be recalled that, as shown in Fig. 7, the $(p_{1/2})^2$ contribution to the 0^+ ground-state transition demonstrates a more marked difference between the sequential and direct processes than does the $(g_{9/2})^2$ contribution. The reactions $^{88}Sr(X,Y)^{90}Zr_{g.s.}$, whose transferred nucleons in the heavy system are largely in the $(p_{1/2})^2$ configuration therefore show a more marked difference between the direct and sequential processes than does the $^{90}Zr(^{16}O,^{14}C)^{92}Mo_{g.s.}$ reaction, whose transferred nucleons in the heavy system are largely in the $(g_{9/2})^2$ configuration.

A small change (5–10%) of the relative probability between different configurations in the present $(p_{1/2}, g_{9/2})$ truncated shell model, was found to introduce little change as far as the general shape of the angular distributions was concerned; nor does such a change effect the magnitude of the calculated cross sections significantly.

Normalization factors: The normalization factors, which are defined by

$$N = \sigma_{exp}/\sigma_{theo},$$

are listed in Table V for the direct and sequential processes, respectively, and for the coherent sum of the two. The normalization factor for the sum of the two processes for each reaction is not much different from that of the sequential process above because the latter cross-section contribution is dominant throughout.

Inclusion of sequential amplitudes clearly improves the absolute normalization by a large factor although the commonly encountered problem[8,9,33,34,36-39] in two-nucleon transfer reactions wherein the theories predict cross sections lower than those observed experimentally persists.

Although Kammuri[8] and Feng[9] have reported satisfactory agreement with experimental data in the case of certain $(^{18}O,^{16}O)$ two-neutron transfer reactions where they have found normalization factors close to 1 (from 0.29 to 2), they both have underestimated the cross sections for the two-proton transfer reactions $(^{16}O,^{14}C)$ by one to two orders of magnitude—similar discrepancies to those observed in our $(^{16}O,^{14}C)$ cases. This rather striking difference in the ^{18}O and ^{16}O induced reactions may reflect the fact that in the former reaction two valence neutrons are being stripped from an ^{16}O core whereas in the latter, the closed core must be broken.

IV. CONCLUSION

We have measured angular distributions for population of low-lying residual states in the reactions

$^{88}Sr(^{16}O,^{14}C)^{90}Zr$, $^{90}Zr(^{16}O,^{14}C)^{92}Mo$, $^{88}Sr(^{12}C,^{10}Be)^{90}Zr$, and $^{90}Zr(^{12}C,^{10}Be)^{92}Mo$ at incident energies $E(^{16}O)_{lab} = 80$ MeV and $E(^{12}C)_{lab} = 60$ MeV and have carried out detailed model calculations for these reactions.

We have demonstrated the importance of including recoil in order to account for the configuration dependence of the DWBA cross sections; we have also shown that sequential amplitudes must be included in the analysis of these heavy-ion two-nucleon transfer reactions. Both the shapes and magnitudes of the calculated angular distributions were found to depend on the microscopic configurations participating in the sequential process. In addition, a significant dependence of the sequential transfer mechanism on the intermediate Q value was observed. Inclusion of sequential processes significantly improves the magnitudes of the calculated cross sections, but large discrepancies between theory and experiment remain nonetheless. The general trends in the angular distributions corresponding to population of the 0^+ residual ground states in the four reactions studied—relative magnitudes, shapes at forward angles and slopes at backward angles—are well understood as reflecting kinematic matching conditions as well as effects associated with the underlying nuclear structure and reaction mechanisms.

We are indebted to Dr. D. L. Hanson, S. K. Korotky, and S. J. Willett for their help with the experimental aspects of this work.

---

*This work was supported in part by the U.S. Department of Energy under Contract No. EY-76-C-02-3074.

†Present address: Bell Telephone Laboratories, Murray Hill, New Jersey.

‡Present address: T. J. Watson Research Laboratories, Yorktown Heights, New York.

[1]M. Toyama, Phys. Lett. 38B, 147 (1972).

[2]R. Schaeffer and G. F. Bertsch, Phys. Lett. 38B, 159 (1972).

[3]W. R. Coker, T. Udagawa, and H. H. Wolter, Phys. Lett. 41B, 237 (1972).

[4]M. Igarashi, M. Kawai and K. Yazaki, Phys. Lett. 42B, 323 (1972).

[5]H. H. Duhm, H. Hafner, R. Renfordt, M. Goldschmidt, O. Dragun, and K. J. Kubo, Phys. Lett. 48B, 1 (1974).

[6]C. Gaarde and T. Kammuri, Nucl. Phys. A221, 238 (1974).

[7]F. Osterfeld and H. H. Wolter, Phys. Lett. 60B, 253 (1976).

[8]T. Kammuri, H. Yoshida and S. Yamaji, in *Proceedings of the International Symposium Structure of Nuclei and Transfer Reactions Induced by Heavy Ions, Tokyo, 1975* edited by H. Kamitsubo, I. Khono, and T. Marumori, (IPCR Cyclotron Progress Report Supplement 4, WAKOSHI, 1975), p. 560; T. Kammuri, Nucl. Phys. A259, 343 (1976).

[9]D. H. Feng, T. Udagawa, and T. Tamura, Nucl. Phys. A274, 262 (1976).

[10]K. A. Erb, D. L. Hanson, R. J. Ascuitto, B. Sorensen, and J. S. Vaagen, Phys. Rev. Lett. 33, 1102 (1974).

[11]I. Talmi and I. Unna, Nucl. Phys. 19, 225 (1960).

[12]S. Cohen, R. D. Lawson, M. H. MacFarlane, and M. Soga, Phys. Lett. 10, 195 (1964).

[13]N. Auerbach and I. Talmi, Nucl. Phys. 64, 458 (1965).

[14]J. Vervier, Nucl. Phys. 75, 17 (1966).

[15]D. H. Gloeckner, M. H. MacFarlane, R. D. Lawson, and F. J. D. Serduke, Phys. Lett. 40B, 597 (1972).

[16]J. B. Ball and J. B. McGrory, Phys. Lett. 41B, 581 (1972).

[17]D. H. Gloecker and F. J. D. Serduke, Nucl. Phys. A220, 477 (1974).

[18]N. Glendenning, in *Proceedings of the International Conference on Reactions Between Complex Nuclei, Nashville, Tennessee, 1974,* edited by R. L. Robinson, F. K. McGowan, J. B. Ball, and J. H. Hamilton (North-Holland, Amsterdam, 1974), Vol. II, p. 137.

[19]The ^{88}Sr targets were prepared in the Wright Laboratory, Yale University, New Haven, Connecticut; the ^{90}Zr targets were purchased from Micro Matter Corporation, Seattle, Washington.

[20]Purchased from Cambridge Thermionic Corporation, Cambridge, Massachusetts.

[21]R. J. Ascuitto and N. K. Glendenning, Phys. Rev. 181, 1396 (1969).

[22]Code LISA, developed by R. J. Ascuitto (unpublished).

[23]G. B. Sherwood and R. J. Ascuitto (unpublished).

[24]P. R. Christensen, I. Chernov, E. E. Gross, R. Stokstad, and F. Videbek, Nucl. Phys. A207, 433 (1973).

[25]J. Bellicard and P. Leconte, Nucl. Phys. A143, 213 (1970).

[26]K. Matsuda, Y. Awaya, N. Nakanishi, and S. Takeda, J. Phys. Soc. Jpn. 33, 298 (1972).

[27]R. M. DeVries, G. R. Satchler, and J. G. Cramer, Phys. Rev. Lett. 32, 1377 (1974).

[28]J. B. French, E. C. Halbert, J. B. McGrory and S. S. M. Wong, in *Advances in Nuclear Physics*, edited by M. Baranger and E. Vogt (Plenum, New York, 1969), Vol. III.

[29]We are indebted to Dr. B. A. Brown, Dr. W. Chung, and Dr. C. King of Michigan State University for their calculation of these spectroscopic amplitudes using the Oak Ridge–Rochester shell model code.

[30]J. Picard and G. Bassani, Nucl. Phys. A131, 636 (1969).

[31]S. Cohen and D. Kurath, Nucl. Phys. A101, 1 (1967).

[32]S. Cohen and D. Kurath, Nucl. Phys. A141, 145 (1970).

[33]B. F. Bayman, Phys. Rev. Lett. 32, 71 (1974).

[34]T. Takemasa, Phys. Lett. 55B, 28 (1975).

[35]R. Bass, Nucl. Phys. A231, 45 (1974).

[36]A. J. Baltz and S. Kahana, Phys. Rev. Lett. 29, 1267 (1972).

[37]L. A. Charlton, Nucl. Phys. A241, 144 (1975).

[38]J. F. Petersen, D. A. Lewis, D. Denhard, H. P. Morse, and B. F. Bayman, Phys. Rev. Lett. 36, 307 (1976).

[39]Y. Eisen, H. T. Fortune, W. Henning, D. G. Kovar, S. Vigdor, and B. Zeidman, Phys. Rev. C 13, 699 (1976).